ACS Chemical Neuroscience

pubs.acs.org/chemneuro
Research Article

Transcriptome-Wide Profiling of Nascent RNA in Neurons with Enriched H3K27ac Signal Elevates eRNA Identification Efficiency

Jiazhi Jiang,○ Sha Liu,○ Ziyue Xu, Shuangqi Yu, Lesheng Wang, Shengrong Long, Shengda Ye, Yu Yan, Hongyu Xu, Jianjian Zhang, Wei Wei,* Qiongyi Zhao,* and Xiang Li*

Cite This: ACS Chem. Neurosci. 2024, 15, 3626−3639
Read Online

ACCESS | Metrics & More | Article Recommendations | Supporting Information

ABSTRACT: Growing evidence suggests that activity-dependent gene expression is crucial for neuronal plasticity and behavioral experience. Enhancer RNAs (eRNAs), a class of long noncoding RNAs, play a key role in these processes. However, eRNAs are highly dynamic and are often present at lower levels than their corresponding mRNAs, making them difficult to detect using total RNA-seq techniques. Nascent RNA sequencing, which separates nascent RNAs from the steady-state RNA population, has been shown to increase the ability to detect activity-induced eRNAs with a higher signal-to-noise ratio. However, there is a lack of bioinformatic tools or pipelines for detecting eRNAs utilizing nascent RNA-seq and other multiomics data sets. In this study, we addressed this gap by developing a novel bioinformatic framework, e-finder, for finding eRNAs and have made it available to the scientific community. Additionally, we reanalyzed our previous nascent RNA sequencing data and compared them with total RNA-seq data to identify activity-regulated RNAs in neuronal cell populations. Using H3K27 acetylome data, we characterized activity-dependent eRNAs that drive the transcriptional activity of the target genes. Our analysis identified a subset of eRNAs involved in mediating synapse organization, which showed increased activity-dependent transcription after the potassium chloride stimulation. Notably, our data suggest that nascent RNA-seq with an enriched H3K27ac signal exhibits high resolution to identify potential eRNAs in response to membrane depolarization. Our findings uncover the role of the eRNA-mediated gene activation network in neuronal systems, providing new insights into the molecular processes characterizing neurological diseases.

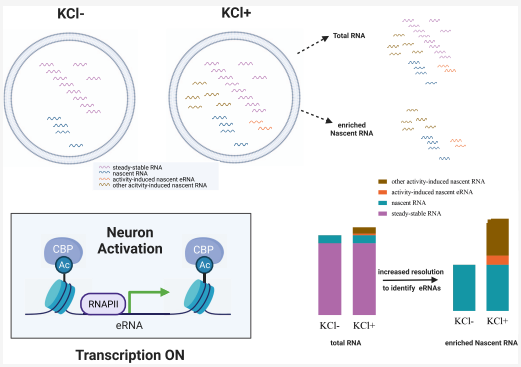

KEYWORDS: *enhancer RNAs, nascent RNA sequencing, e-finder, H3K27ac, activity-dependent eRNAs, neuronal systems*

INTRODUCTION

The long-range looping interactions among enhancers and target genes in the nervous system are crucial for activity-dependent gene expression during neural plasticity, learning, and memory formation.[1−3] Enhancers are DNA sequences that regulate gene expression in a cell-type- and state-specific manner. Enhancer RNAs (eRNAs), transcribed from enhancer elements, can influence gene expression through chromatin looping, and a large amount of enhancer−promoter loopings mediated by eRNAs are established in a state-specific manner.[1,4,5] Active eRNAs that regulate transcription levels are described as elements enriched for transcription factors and histone modifications, such as cAMP response element-binding protein (CBP), histone H3 monomethylated at lysine 4 (H3K4me1), and histone H3 lysine 27 acetylation (H3K27ac).[5−9] One challenge in detecting changes in eRNA expression induced by activity lies in their inherent instability. Due to their short length (approximately 200nt to 2 kb) and sensitivity to RNA exosome-mediated degradation,[10] eRNAs may evade detection by total RNA-seq. This limitation underscores the need for techniques that can detect nascent RNA in aqueous RNA prior to eRNA degradation.

Nascent RNAs, newly synthesized RNA molecules undergoing active transcription, can be identified through a variety of sequencing-based methods. One straightforward technique involves the use of strong washes to isolate RNA attached to chromatin, leveraging the stability of the nascent RNAs and polymerase during chromatin salt fractionation.[11] While this method enriches nascent RNA, it can also capture mature RNAs associated with chromatin. To improve the specificity, native elongating transcript sequencing (NET-seq) was developed.[12,13] NET-seq isolates RNA associated with Pol II through immunoprecipitation but can still capture some non-nascent RNAs that stably bind to Pol II, including small

Received: January 20, 2024
Revised: August 17, 2024
Accepted: August 19, 2024
Published: October 8, 2024

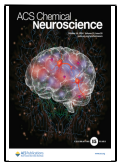

https://doi.org/10.1021/acschemneuro.4c00047
ACS Chem. Neurosci. 2024, 15, 3626−3639

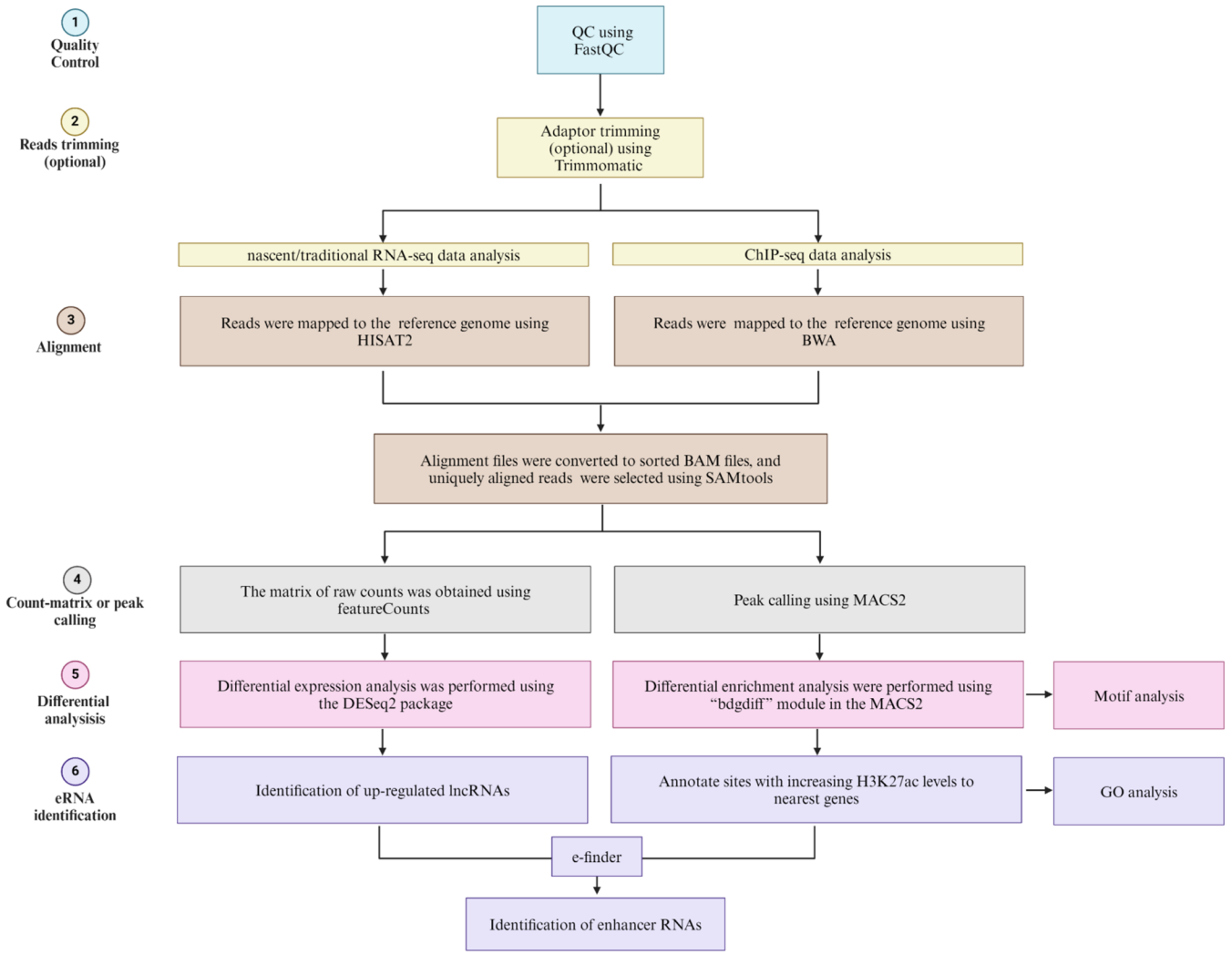

Figure 1. Flow diagram of the e-finder illustrating the framework of enhancer RNA identification.

nuclear RNAs.[14] As an alternative, run-on assays, which capture RNAs undergoing synthesis, use an anionic detergent sarkosyl to remove proteins from chromatin, allowing Pol II to progress along the genome in vitro.[15,16] However, these assays can potentially distort Pol II's conformation.[17]

In contrast to these methods, metabolic labeling experiments differ in their approach by using modified, cell-permeable nucleosides and require at least 5 min for these nucleosides to be converted into UTPs.[18,19] However, these methods do not offer cell-type specificity. To address this limitation, Zajaczkowski et al. adopted the UPRT−5EUracil method for profiling activity-regulated nascent RNAs within specific neuronal cell populations.[20] This approach notably improved the enrichment of stimulus-responsive transcripts for transcriptome-wide expression profiling.[20] Leveraging this data set, we combined genome-wide enhancer elements enriched for H3K27ac with neuron-specific nascent RNA-seq data to explore eRNA-mediated gene expression patterns in cortical neurons under two distinct activation conditions. To model neuronal activation, we used potassium chloride (KCl) treatment to mimic neuronal activity in primary cortical neurons. This is a well-established system that can activate various neuronal subtypes and recapitulate most cellular and transcriptional processes in neurons responding to physiological stimulation in vivo. Neuronal activation may be initiated by calcium influx through voltage-sensitive calcium channels (VSCCs) and ligand-gated ion channels, such as the *N*-methyl-D-aspartate-type (NMDA), or by intracellular calcium release.[21,22] Research has particularly highlighted that calcium influx through L-type VSCCs (L-VSCCs) preferentially drives gene transcription.[22] This is likely due to the proximity of L-VSCCs to the nucleus and their specific calcium conductance and gating characteristics.[22−24] Notably, L-VSCCs play a major role in mediating the effects of elevated extracellular KCl.[25] Employing the KCl activation model to explore activity-induced genes enhances our understanding of memory-associated cellular mechanisms and the behavior of activated neurons during learning processes. We discovered a subset of active enhancers in intronic regions linked to genes involved in synapse organization and neuronal connectivity. In addition, we identified 26 eRNA−mRNA pairs as potential regulatory links in eRNA and gene interactions. Furthermore, we developed a novel bioinformatic framework, e-finder, to identify eRNAs, and we have made it available to the scientific community. Our study underscores that nascent RNA-seq enhances the sensitivity in detecting eRNAs in neurons and may aid in uncovering the eRNA function in neural plasticity.

https://doi.org/10.1021/acschemneuro.4c00047
ACS Chem. Neurosci. 2024, 15, 3626−3639

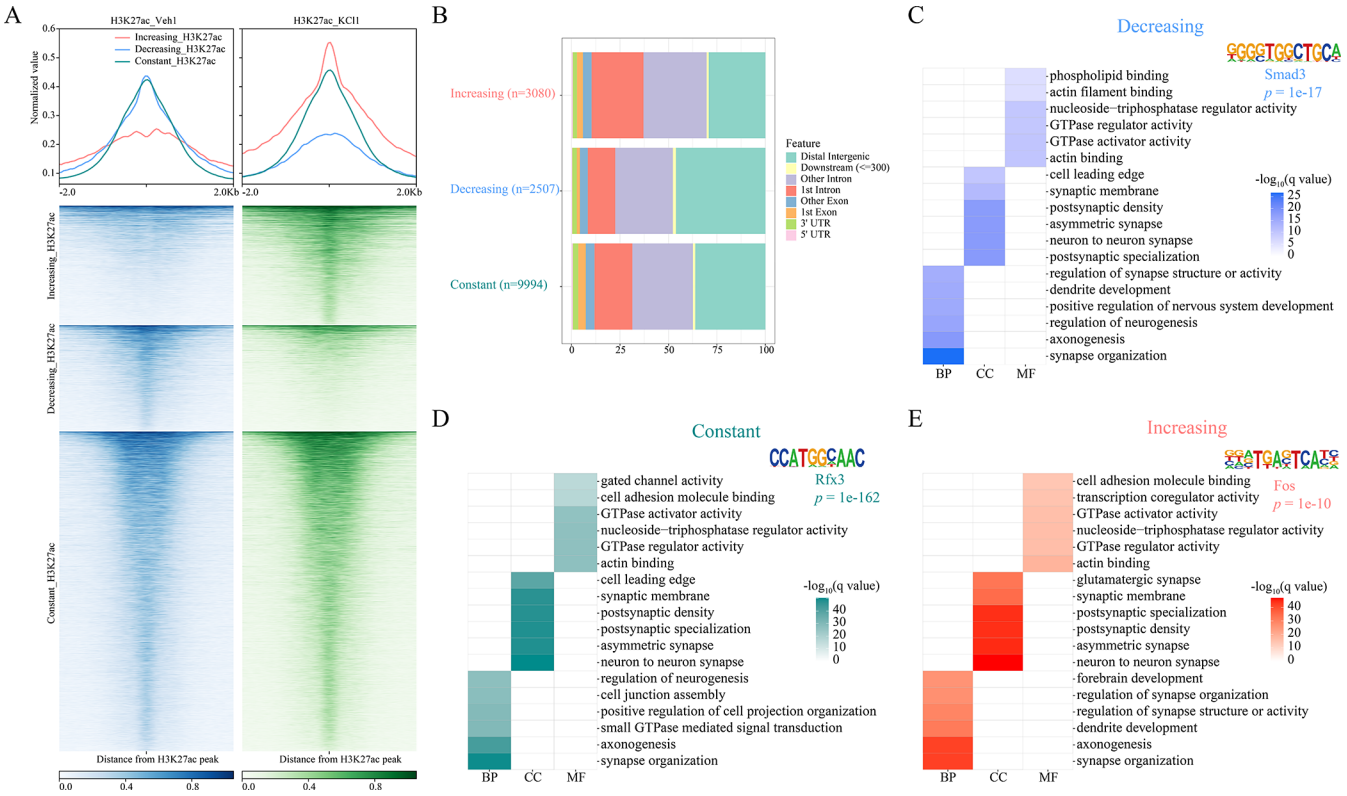

Figure 2. Identification and characterization of potential enhancer loci. (A) Metagene plots and heatmap of H3K27ac at differential H3K27ac sites in response to neuronal activity. (B) Genomic distribution of differential H3K27ac peaks. (C−E) Heatmap shows -log10(q-value) of the GO term enrichment analysis of genes related to (C) decreasing, (D) constant, and (E) increasing H3K27ac peaks (left). DNA motif enrichment analysis at differential H3K27ac sites indicates different transcription factor enrichment in response to neuronal activity (right). Representative examples of transcription factor were displayed. 17, 29, and 25 TFs were found using decreasing, constant, and increasing H3K27ac peaks, respectively. BP, biological processes; CC, cellular component; and MF, molecular function.

RESULTS

Enhancer RNA Finder (e-Finder). The enhancer RNA finder (e-finder) consists of six steps (Figure 1). Step 1 involves performing quality control to assess the quality of the FASTQ files of nascent or total RNA-seq and ChIP-seq Step 2, an optional step, trims reads with adaptors and low-quality reads. In Step 3, reads of nascent or total RNA-seq and ChIP-seq after quality control are aligned to the reference genome, and uniquely aligned reads are chosen for quantification or peak calling. For RNA-seq in Step 4, quantification is performed to obtain a matrix of raw counts, while the H3K27ac enriched sites under two conditions are obtained by peak calling. Step 5 includes differential expression analysis to obtain upregulated lncRNAs and differential enrichment analysis to obtain sites with elevated H3K27ac levels after KCl stimulation. Finally, in Step 6, upregulated lncRNAs annotated by sites with elevated H3K27ac levels are identified as potential eRNAs, and bioinformatic prediction of eRNA−mRNA pairs is performed. e-finder is available through the GitHub page (https://github.com/jz-Jiang/e-finder).

Genome-Wide Identification and Characterization of Activity-Dependent Enhancer Loci. The genome-wide analysis of chromatin modifications reveals that H3K27ac is a common feature of enhancer loci.[4,5] Therefore, in this study, we defined putative activity-dependent enhancer sites using the following criteria: (i) regions enriched for H3K27ac signals in response to KCl stimulation, (ii) regions located at least 1 kb away from annotated TSSs of mRNAs, and (iii) regions not overlapping with the ENCODE mm10 blacklist regions. Following these criteria, we identified H3K27ac peaks based on the H3K27ac ChIP-seq data and classified them into three categories: decreasing, constant, and increasing H3K27ac peaks in response to KCl stimulation compared to the control group. In total, we identified 2,726, 8,294, and 3,074 H3K27ac peaks for the decreasing, constant, and increasing categories, respectively (Figures 2A and S1A). We verified H3K27ac enrichment at target regions using two additional H3K27ac ChIP-seq data sets (Figures 2A and S1A−C). Notably, H3K27ac enrichment at increasing sites could be seen across the three data sets derived from three different time points (45 min, 2 h, and 24 h) and two neuronal stimulating conditions (KCl and bicuculline, a GABAA-receptor antagonist). This indicates that neuronal activation, regardless of the duration or types of signaling, stably induces H3K27ac enrichment at genes that are crucial for synapse plasticity or dendrite function.

To further investigate the distribution of genomic locations for these peaks in each category, we annotated each peak with its corresponding genomic feature, including promoter, 5′UTR, 3′UTR, first exon, other exons, first intron, and other introns, downstream of the gene body, and distal intergenic regions (Figure 2B). Notably, significant portions of H3K27ac peaks are in intron and distal intergenic regions. Interestingly, we noticed that the proportion of H3K27ac peaks in intron regions (i.e., first intron and other introns) gradually increased in the three categories in response to membrane depolarization, with the percentages for decreasing,

https://doi.org/10.1021/acschemneuro.4c00047
ACS Chem. Neurosci. 2024, 15, 3626−3639

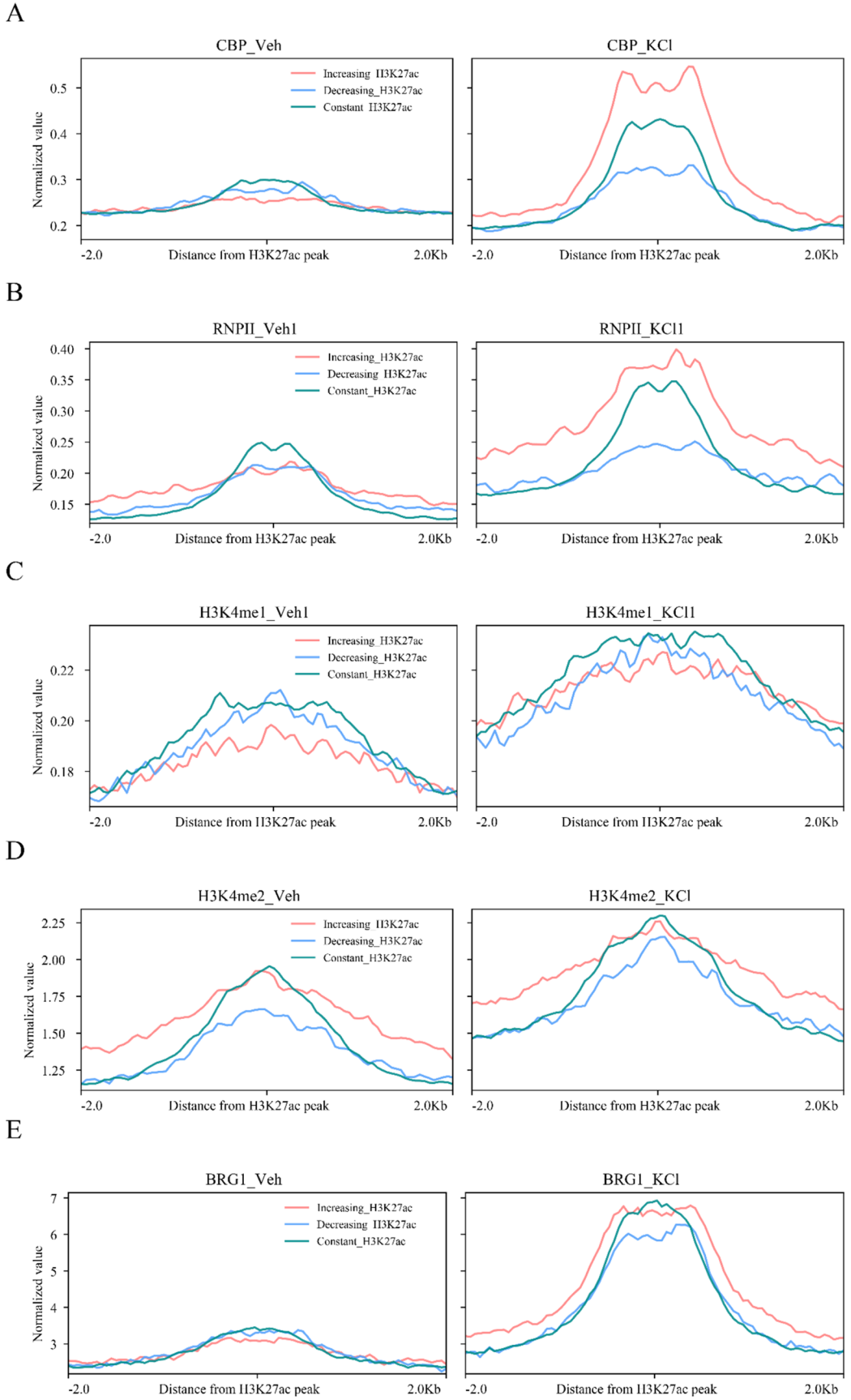

Figure 3. Comparison of binding profiles at differential H3K27ac sites. (A–E) Binding profiles of CBP, RNAPII, and BRG1 and multiple histone modifications at differential H3K27ac sites in response to neuronal activity. Increasing H3K27ac sites show higher enrichment for active enhancer markers, including CBP, RNAPII, and BRG1, in response to KCl stimulation but not the H3K4me1 and H3K4me2 modifications. Veh indicates vehicle-treated controls.

https://doi.org/10.1021/acschemneuro.4c00047
ACS Chem. Neurosci. 2024, 15, 3626−3639

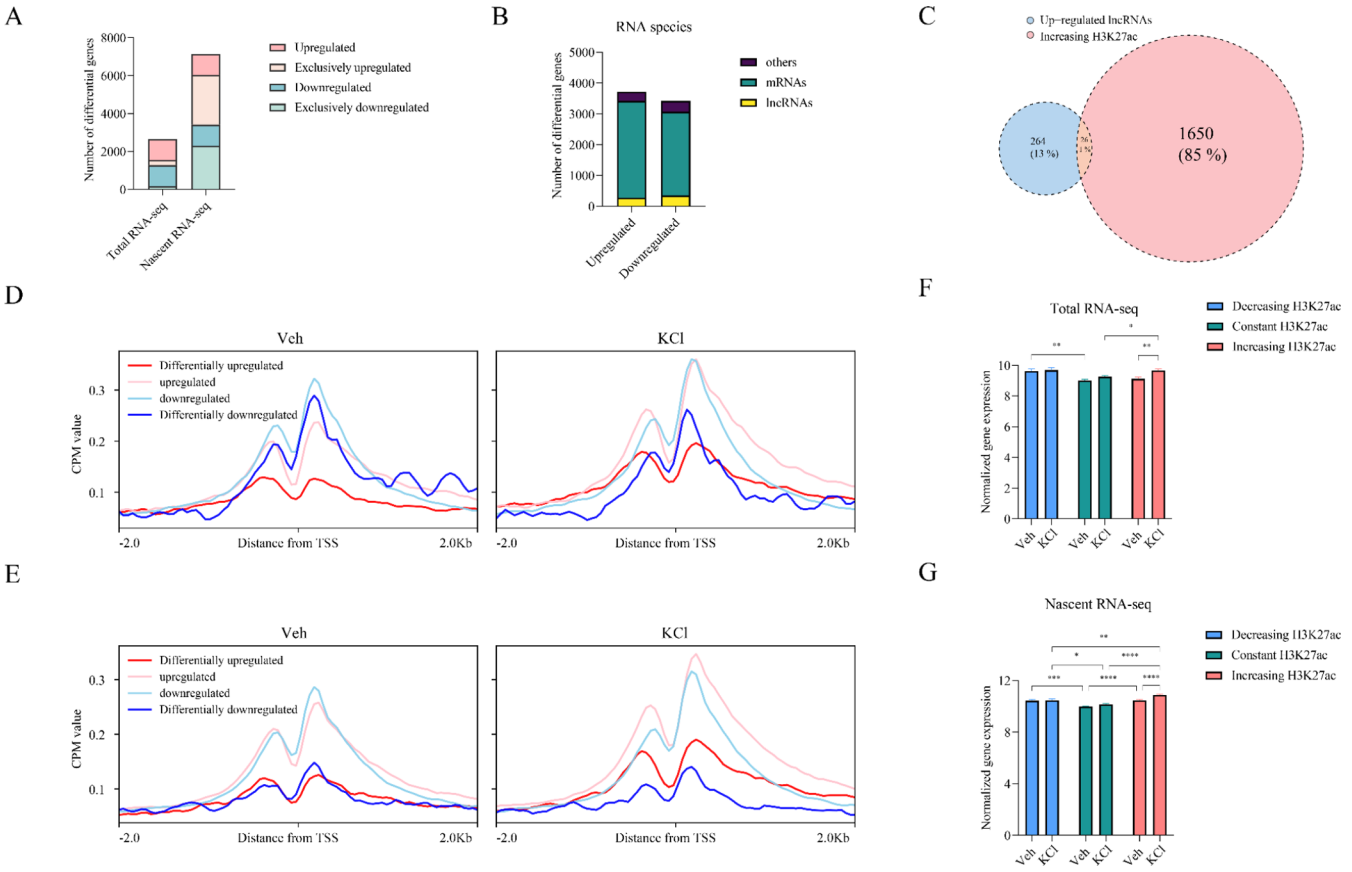

Figure 4. H3K27ac enrichment correlates with the transcription of eRNAs. (A) Bar plots show the number of differential genes at two activity states (Veh vs KCl) detected by total RNA-seq and nascent RNA-seq. Exclusively upregulated and exclusively downregulated indicate up- or downregulated genes specifically from total or nascent RNA-seq, respectively. Upregulated or downregulated indicates up- or downregulated genes detected by both total and nascent RNA-seq, respectively. (B) Bar charts depicting the frequency of different classes of RNA species enriched by nascent RNA-seq. (C) The Venn diagrams summarize the number of upregulated lncRNAs enriched for H3K27ac. (D) H3K27ac occupancy profile at genes from total RNA-seq. (E) H3K27ac occupancy profile at genes from nascent RNA-seq. Differentially upregulated, upregulated, downregulated, and differentially downregulated are defined when genes with FDR < 0.05 and LogF C > 1.5, 0 < Log FC ≤ 1.5, − 1.5 ≤ Log FC < 0, Log FC < − 1.5 in the comparison of KCl vs veh, respectively. LogFC indicates log fold change in gene expression in neurons treated with KCl versus Veh. (F) Normalized expression of genes annotated by the corresponding H3K27ac at two activity states from total RNA-seq (n = 200−726 genes per group, 2-way ANOVA, $F(2, 2782) = 10.06$, Tukey's multiple comparison test). (G) Normalized expression of genes annotated by the corresponding H3K27ac at two activity states from nascent RNA-seq (n = 650−2184 genes per group, 2-way ANOVA, $F(2, 8146) = 58.80$, Sidak's multiple comparisons). Error bars represent SEM, *p < 0.05, **p < 0.01, ***p < 0.001, ****p < 0.0001.

constant, and increasing categories being 41.68%, 43.43%, and 50.27%, respectively. Meanwhile, the proportion of H3K27ac peaks in distal intergenic regions gradually decreased, with the decreasing, constant, and increasing categories being 42.57, 31.41, and 24.57%, respectively (Figure 2B).

To determine which transcription factor binding sites are enriched in each H3K27ac category, we conducted a DNA motif enrichment analysis. GO enrichment analysis was also performed on genes correlated with the corresponding H3K27ac peaks to investigate the biological processes affected by the H3K27ac levels. Sites with increasing, decreasing, and constant H3K27ac levels were found to be associated with genes involved in synapse organization and neuronal connectivity (Figure 2C−E). Sites with increasing H3K27ac levels showed enrichment in binding motifs for Fos family proteins that are robustly induced by neuronal activity (Figure 2E).[8,26,27] Sites with decreasing H3K27ac levels were enriched in binding motifs for Smad3, a crucial regulator of neuroprotection and synaptogenesis in neuronal signaling pathways (Figure 2C).[28,29] Sites maintaining constant H3K27ac levels showed significant enrichment for motifs bound by transcription factor Rfx3, which acts as a master regulator of the central nervous system development and is involved in the pathogenesis of neurodevelopmental disease (Figure 2D).[30]

We assessed the enhancer loci with transcriptional cofactor, polymerase, and histone modification markers, including CBP, RNAPII, H3K4me1, H3K4me3, and H3K27me3. The binding profiles showed that increasing H3K27ac sites were enriched for active transcription markers, including CBP and RNAPII, in response to KCl stimulation but not for the promoter marker H3K4me3 and repressive H3K27me3 modification (Figures 3A,B and S2A−E). CBP enrichment was also exhibited at decreasing and constant H3K27ac sites, although the signal increased most significantly at increasing H3K27ac sites after KCl treatment (Figure 3A). Notably, the H3K4me1 signal remained stable between KCl treatment and the vehicle conditions (Figures 3C and S2F). This aligns with the roles of H3K4me1 and H3K27ac in enhancer activation: the pre-existing H3K4me1 is essential for potential poised/primed enhancers for later activation by acquiring H3K27ac.[31,32] However, emerging evidence indicates that the high levels of RNAPII occupancy can be used to define the active

https://doi.org/10.1021/acschemneuro.4c00047
ACS Chem. Neurosci. 2024, 15, 3626−3639

enhancers.[5,33] We found more enrichment of RNAPII at increasing H3K27ac sites in response to KCl (Figures 3B and S2A), indicating activity-regulated eRNA transcription and suggesting that increased H3K27ac occupancy is a better predictor of enhancer activity than H3K4me1. Furthermore, we included two additional enhancer markers, H3K4me2[34] and BRG1,[35] to confirm the reliability of using increasing H3K27ac loci for identifying enhancers (Figure 3D,E). To test the broader applicability, we applied e-finder to Reelin-treated data, another neuronal activation method by triggering the proteolytical processing of its receptor LRP8 bidirectionally regulated by the activation of the NMDA-receptor signaling.[36] Consistent with the results from the KCl stimulation model, sites enriched with H3K27ac in response to Reelin treatment also exhibited CBP and CREB enrichment but not H3K4me2 (Figure S3A−D). These findings demonstrate that the approach for identifying activity-dependent enhancers is effective and reliable, which can be applied to other activation models and different cells or cell lines.

Identification and Characterization of Activity-Dependent Enhancer RNAs. To determine whether activity-dependent enhancers are correlated with RNA synthesis, we analyzed nascent RNA-seq and traditional total RNA-seq data to examine dynamic changes in enhancer-mediated gene regulation. The results showed that nascent RNA-seq significantly improved sensitivity in detecting stimulus-regulated transcripts, including up- and downregulated lncRNAs, compared to total RNA-seq (Figure 4A and Tables S2 and S3). We identified 7135 activity-regulated genes, of which 4933 were not included in the differentially expressed gene list of total RNA-seq profiling (Figure 4A). In particular, we detected 290 upregulated lncRNAs (Figure 4B). By assigning peaks to proximal genes and excluding distal intergenic genes, we obtained 1676 genes enriched with H3K27ac. By overlaying the H3K27ac data, we identified 26 upregulated lncRNAs that exhibited increased H3K27ac signal in response to KCl (Figure 4C and Table S4). Next, we examined the H3K27ac occupancy profile at differential genes from total or nascent RNA-seq and found that H3K27ac is enriched at the TSS of upregulated genes after KCl treatment but not for downregulated genes, confirming that H3K27ac is an active histone modification (Figure 4D,E).

To compare the capability of total RNA-seq and nascent RNA-seq in the detection of eRNAs, we assigned three categories of H3K27ac peaks to the closest genes and obtained expression data from total and nascent RNA-seq, respectively. We found that genes annotated by increasing the number of H3K27ac sites from total RNA-seq responses to KCl stimulation (Figure 4F). However, genes detected by nascent RNA-seq that showed upregulated expression and enrichment of the H3K27ac signal upon membrane depolarization might be putative eRNAs (Figure 4G). Compared to genes annotated by decreasing and constant H3K27ac sites, genes annotated by increasing H3K27ac sites are significantly upregulated when KCl stimulation was applied but not for untreated cells (Figure 4G). In addition, the expression of the gene annotated by increasing H3K27ac was higher than that of genes annotated by decreasing and constant H3K27ac after KCl treatment. These results demonstrated that nascent RNA-seq achieved higher sensitivity in detecting eRNA candidates than total RNA-seq. Taken together, these findings indicate that the enrichment of H3K27ac, which functions as activity-regulated enhancers, is associated with increased transcription and that nascent RNA-seq exhibits high resolution in detecting eRNAs by separating nascent RNA from steady-state RNA populations.

To verify the importance of nascent RNA-seq in identifying eRNA, we applied e-finder to H3K27ac ChIP-seq and RNA-seq data from day 10 neurons treated with NMDA. We identified regions with increasing, constant, and decreasing H3K27ac levels in response to NMDA treatment. Similar to KCl stimulation, we found that NMDA-related H3K27ac peaks were primarily enriched in intronic regions (Figure S4A). The percentages of increasing, constant, and decreasing H3K27ac_NMDA located in the intronic regions were 50.37, 40.30, and 44.74%, respectively (Figure S4A). GO analysis of genes annotated with the three categories of NMDA-related H3K27ac peaks revealed that NMDA-induced H3K27ac is predominantly distributed at synapse-related genes (Figure S4B−D). However, only 11 peaks (<1%) were enriched with H3K27ac in response to both KCl and NMDA (Figure S4E), suggesting that while both KCl and NMDA promote H3K27ac enrichment at synapse-related genes, the signaling pathways and responsive genes differ between the two stimuli.

For eRNA identification, we analyzed NMDA-induced total RNA-seq data and identified 1560 upregulated and 1945 downregulated genes (Figure S4F). We then intersected 17 upregulated lncRNAs with genes annotated with increasing H3K27ac_NMDA and found no eRNA. There are two explanations for this result: first, since samples were collected 6 h after NMDA treatment, the inherent instability of eRNA may lead to the loss of most eRNA information; second, the total RNA-seq used for the identification exhibited low sensitivity for detecting eRNA, emphasizing the advantage of nascent RNA-seq in identifying eRNA.

The Bioinformatic Prediction of eRNA−mRNA Pairs. To further investigate the dynamic relationship between eRNAs and activity-regulated mRNAs, we focused on 26 upregulated lncRNAs enriched for H3K27ac signals. We performed a Pearson correlation analysis of gene expression between these 26 putative eRNAs and all annotated mRNAs to predict eRNA and its target mRNA pairs. The eRNA−mRNA pairs were selected based on the following criteria: prioritize identifying the mRNA with a correlation greater than 0.8 with the eRNA and closest to the eRNA. If there are no such mRNAs on the same chromosome, select the mRNA with the highest correlation to eRNA (Table 1).

To validate the predicted enhancer-gene regulatory links, we chose four eRNA−mRNA pairs to perform a time-course experiment (Figure 5A). *Arc*, an immediate early gene (IEG),[37] was chosen to verify the activity-dependent gene transcription triggered by KCl depolarization (Figure 5B). Time-course qPCR showed that eRNAs exhibited correlated expression patterns to mRNAs. Furthermore, eRNAs were upregulated earlier than or simultaneously with the expression of target mRNAs in response to membrane depolarization (Figure 5C−F). Interestingly, we discovered that one of the eRNAs, *Gm*40477, was an annotated *Fos* eRNA,[38] demonstrating the efficiency of e-finder. Our results showed that the expression of *Gm*40477 was induced by KCl treatment but peaked with *Fos* mRNA simultaneously, similar to *Sox2ot* and *Pvt*1. We did not observe that *Pvt*1, *Sox2ot*, and *Gm*40477 peaked earlier than correlated mRNA, which may be due to the total RNA used for RT-qPCR analysis instead of nascent RNA. However, this does not affect the correlation between these putative eRNAs and mRNAs, and the biological function of these eRNAs should be

https://doi.org/10.1021/acschemneuro.4c00047
ACS Chem. Neurosci. 2024, 15, 3626−3639

Table 1. eRNAs and Their Putative mRNA Targets

eRNAs	mRNAs	pval	Cor	distance (Kb)
Gm40477	*Fos*	5.63364×10^{-11}	0.922	37.6
Pvt1	*Efr3a*	2.98912×10^{-07}	0.829	3408.9
Sox2ot	*Zmat3*	1.5556×10^{-07}	0.840	1738.3
Gm17750	*Cox7c*	5.022×10^{-16}	0.972	1980
1600020E01Rik	*Snrpg*	1.07543×10^{-07}	0.845	146.9
2410006H16Rik	*Ubb*	1.60588×10^{-13}	0.954	49.664
2610203C22Rik	*Arid5a*	1.43801×10^{-06}	0.802	26676.6
2610307P16Rik	*Sinhcaf*	8.75454×10^{-08}	0.848	No[a]
5330434G04Rik	*Taf1*	1.48856×10^{-06}	0.801	3746.5
B230216N24Rik	*Pam*	5.89792×10^{-07}	0.818	0
BC037704	*Frat2*	2.05043×10^{-07}	0.835	1827
C230034O21Rik	*Fat4*	1.48423×10^{-17}	0.980	−1.3
D830036C21Rik	*Fosb*	9.86752×10^{-08}	0.846	10.1
Dleu2	*Lats2*	1.30224×10^{-06}	0.804	3844.5
G630016G05Rik	*Aldh8a1*	1.39851×10^{-05}	0.753	No
Gm15601	*Nrg3*	6.03433×10^{-08}	0.853	6090.7
Gm17501	*Pdlim5*	1.45819×10^{-07}	0.840	3254.6
Gm26887	*Krt6a*	5.97898×10^{-07}	0.818	No
Gm30541	*Ina*	7.07753×10^{-07}	0.815	6295.3
Gm3294	*Lrrc4*	1.31497×10^{-08}	0.872	149.9
Gm34307	*Ntrk2*	1.19597×10^{-06}	0.805	10.3
Gm34354	*Ntrk2*	4.41937×10^{-08}	0.857	11.9
Lncpint	*Mest*	1.17886×10^{-06}	0.806	334.1
Mir670hg	*Hsd17b12*	9.7973×10^{-09}	0.876	2.7
Mir9−3hg	*Abhd2*	3.26487×10^{-07}	0.828	134.5
Neat1	*Sf1*	5.527×10^{-09}	0.882	518.2

[a]eRNAs and corresponding target mRNAs located on different chromosomes.

addressed in future studies. Overall, these data demonstrate that nascent RNA-seq exhibits high resolution to identify potential eRNAs in contexts such as the response to membrane depolarization.

DISCUSSION

During learning, memory, and behavior, neuron activity is induced through specific calcium-dependent signaling cascades. This activation leads to activity-dependent gene expression, which is regulated by enhancers. Enhancers can be functioned as cis and trans-acting DNA regulatory elements that promote the transcriptional production of target genes, playing important roles in regulating neuronal survival, synapse development, and synaptic plasticity.[4,5,39] Enhancers are characterized by particular features, including CBP occupancy and the enrichment of histone modifications such as H3K4me1 and H3K27ac.[5] However, the activity state of enhancers that share these features is dynamic and limited to specific cell types and genomic contexts.[5] Enhancer activity can be induced by the enrichment of CBP, H3K4me1, and H3K27ac recruited upon membrane depolarization, leading to the elevation of RNA synthesis at enhancers, which is crucial for distinct genetic programs and biological functions.[6,38] Some eRNAs have been reported to function in interacting with RNAPII, various transcription factors, and cofactors to promote gene expression by regulating increased recruitment of transcriptional regulators at enhancers.[40−42] Furthermore, eRNAs play an important role in stabilizing enhancer−promoter looping and directing chromatin-remodeling events to regulate gene expression.[43,44]

Importantly, eRNAs are crucial for the activation of neuronal IEGs following neuronal activation. They facilitate the transition from paused RNAPII to productive elongation.[6,45] Moreover, activity-induced Fos preferentially binds to distinct enhancer repertoires rather than promoters, which drives the cell-type specific regulation of gene expression in response to neuronal activity.[22] This suggests that eRNAs not only play a significant role in initiating and elongating IEG transcription but also mediate the cell-specific activation of gene transcription by IEGs. In addition to playing a significant role under physiological conditions, the expression of eRNAs is also associated with the onset and progression of neurological diseases. Alzheimer's disease pathogenesis is intricately linked to brain-derived neurotrophic factor (BDNF) pathway dysregulation.[46] Within the BDNF-interacting intergenic regions, two eRNAs have been identified as regulators of BDNF expression, underscoring their involvement in the development of neurodegenerative disorders.[47] Additionally, genetic variants related to Parkinson's disease (PD) are predominantly found in noncoding regions, particularly active enhancers.[48] Notably, PD-related variants on chromosome 17q21 appear to cis-regulate an enhancer RNA in dopamine neurons,[48] highlighting its potential as a diagnostic biomarker and therapeutic target for PD. Therefore, overall, studying the regulatory mechanisms of eRNAs under neuronal activation or pathological conditions plays an important role in our understanding of neuronal behavior in memory and the onset and progression of psychiatric diseases.

While it is important to understand how eRNAs contribute to gene expression during neuronal activation, their identification poses a challenge, as they are not easily detected by traditional total RNA-seq profiling. To overcome this issue, we utilized nascent RNA sequencing data, which label nascent RNAs with the UPRT−5EUracil system, to identify activity-dependent eRNAs and predict potential eRNA−mRNA interactions. First, we identified active enhancers that showed the enrichment of H3K27ac in response to membrane depolarization. Our analysis revealed that while some enhancers are located in intergenic regions, a considerable proportion is situated within gene bodies, particularly intronic regions, consistent with previous studies.[4,49] Enrichment of H3K27ac drives the transcription of activity-regulated genes and recruits transcription factor Fos, which plays an important role in activity-dependent enhancer function and drives a large subset of genes crucial for neuronal activity.[8,26,38,50] Our results demonstrate that the enrichment of H3K27ac recruits Fos upon membrane depolarization to drive the second wave of transcription of activity-regulated genes, many of which encode products that are localized or act at synapses. Active enhancers enriched for H3K27ac also showed increased occupancy of CBP and RNAPII in response to KCl, highlighting the importance of H3K27ac for the identification of enhancers and suggesting that RNAPII might be a better marker of enhancer activity. We observed that the intensities of H3K4me3 at increasing H3K27ac sites did not increase with KCl treatment. Previous ChIP-seq studies have shown that H3K4me3 signals are typically detected as sharp peaks (<1 kb) located around TSSs and are often associated with gene activation.[51] However, broad H3K4me3 signals (>4 kb) have also been identified within the gene body of a small subset of genes that display enhanced transcription.[51,52] In this study, we examined H3K27ac sites located outside of the TSSs and found that the H3K4me3 signals at these sites may represent broad peaks.

https://doi.org/10.1021/acschemneuro.4c00047
ACS Chem. Neurosci. 2024, 15, 3626−3639

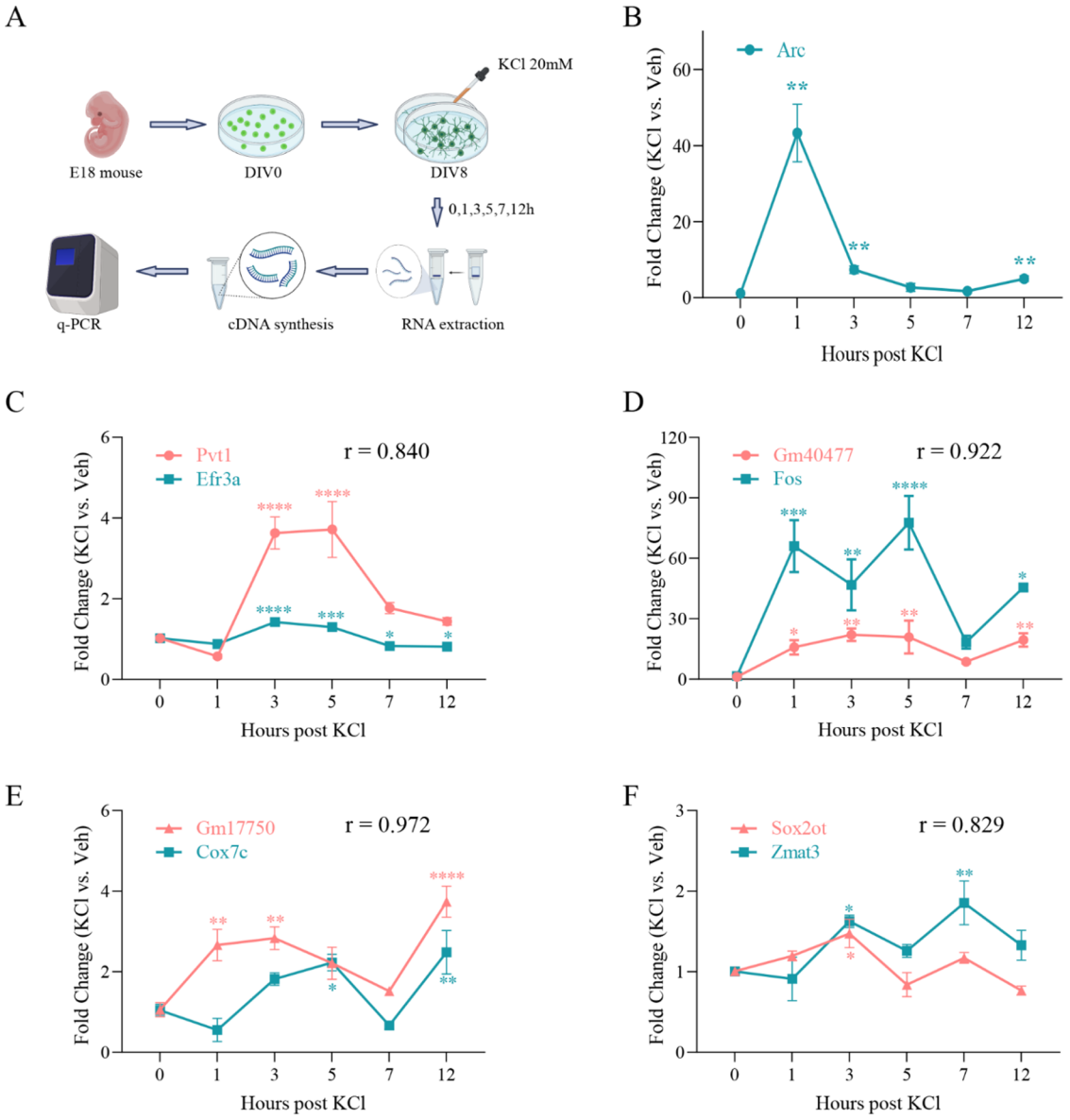

Figure 5. Activity dependence of eRNAs and mRNAs. (A) Illustration of the primary cultured cortical neuron preparation used to RT-qPCR. (B) Time-course qPCR of *Arc* upon neuronal depolarization, one-way ANOVA, F (1.090, 8.503) = 49.29, Holm−Šídák's multiple comparison test. (C−F) Time-course qPCR of four eRNAs and corresponding target mRNAs upon neuronal depolarization, respectively, one-way ANOVA with Dunnett's multiple comparison test, *Pvt*1: F (5, 24) = 16.04; *Efr3a*: F (5, 25) = 21.69; *Gm*40477: F (5, 22) = 4.958; *Fos*: F (5, 24) = 9.467; *Gm*17750: F (5, 23) = 10.32; *Cox7c*: F (5, 26) = 9.034; *Sox2ot*: F (5, 23) = 6.440; *Zmat*3: F (5, 25) = 4.453. Light pink represents eRNAs, and dark cyan represents target mRNAs. *p < 0.05; **p < 0.01; ***p < 0.001, ****p < 0.0001; Error bars represent SEM (n = 4−6 biological replicates per group).

It is possible that downstream H3K4me3 nucleosomes, when in the highly acetylated state, contribute to enhanced transcription by maintaining an atypical nucleosome structure known as the U-shaped nucleosome, rather than through an intensity-dependent mechanism.[51] This may explain why we observed similar levels of H3K4me3 enrichment at increasing H3K27ac sites under both control and KCl-treated conditions.

Nascent RNA-seq, which enriches for nascent RNA prior to sequencing, dramatically improves the ability to detect nascent RNAs and enables the uncovering of the gene regulatory network in neurons compared to traditional total RNA-seq.[10] The UPRT−5EUracil system[20] used in our nascent RNA-seq technology is more suitable for profiling transcriptome-wide expression patterns in neurons due to their complicated and activity-dependent transcription. By combining this nascent RNA-seq with ChIP-seq of H3K27ac, we were able to detect 26 potential eRNAs, and RT-qPCR throughout a time series suggested that eRNA transcription peaked earlier or simultaneously with the expression of target mRNAs in response to membrane depolarization. Surprisingly, of the 1676 sites enriched for H3K27ac, only 26 showed enhanced transcription. While the reasons for this were not explored in this study, the relatively lower concentration of KCl used in nascent RNA-seq may partly explain this. H3K27ac is reported to accumulate at enhancers through the eRNA-mediated catalytic activity of the histone acetyltransferase CBP.[5] Emerging evidence shows that H3K27ac can accumulate at enhancers despite blocking eRNA induction and RNAPII recruitment,[53] suggesting that there might be other mechanisms regulating H3K27ac deposition and eRNA induction.

https://doi.org/10.1021/acschemneuro.4c00047
ACS Chem. Neurosci. 2024, 15, 3626−3639

Our results demonstrate that the nascent RNA-seq with the UPRT−5EUracil system enables the exploration of how eRNAs contribute to gene regulation and function in the context of neuronal activation.

Interestingly, we noticed that *Pvt*1, one of the eRNAs enriched for H3K27ac, CBP, and RNAPII in response to membrane depolarization, exhibits a consistent change in the pattern expression with *Efr*3*a*. Previous studies have not explored the interactions between *Pvt*1 and *Efr*3*a* in the neuronal system, likely due to the relatively large distance (about 3Mb) between them. *Pvt*1 has been reported as a stabilizer of the Myc protein as well as an epigenetic enhancer of the *Myc* gene in several tumor types.[54−56] Furthermore, *Pvt*1 inhibition may direct learning and memory in epilepsy by driving the BDNF expression in the hippocampus.[57] Efr3a, a critical plasma membrane protein, plays an essential role in many functions at the neuron synapse.[58] Hippocampal neurogenesis can be triggered by brain-specific deletion of *Efr*3*a*, presumably through the BDNF-TrkB signaling pathway.[59] Given that inhibition of either *Pvt*1 or *Efr*3*a* is involved in upregulating BDNF, it is possible that *Pvt*1 regulates *Efr*3*a* as an eRNA, thereby controlling BDNF, which needs further investigation.

3C-based technologies have provided new insights into the 3D genome structures and visualizing interaction rates between particular active enhancers and target genes.[60,61] These technologies have allowed the quantification of the large-scale spatiotemporal interactions among genomic loci and have demonstrated that the mammalian genome folds into higher-order chromatin domains, including chromosomal compartments A/B,[61] topologically associating domains (TADs),[62] and long-range looping interactions.[63] Most long-range looping interactions occur within the same TAD, and enhancers within each megabase-sized TAD are thought to communicate with promoters through chromatin looping. Future studies will investigate whether dynamic enhancer−promoter communication between these eRNAs and target mRNAs is established within the same TADs in response to membrane depolarization to function in learning, memory, and behavior.

One caveat in this study is that the ChIP-seq data sets of multiple histone modifications (H3K27ac, RNAPII, CBP, H3K4me1, H3K27me3, and H3K4me3) from primary mouse neurons treated with either vehicle or 55 mM KCl for 2 h were not obtained under the same conditions as the nascent RNA-seq data (20 mM KCl for 3 h). Gene expression profiles under neuronal activation can be classed into two waves.[53,64] The first wave consists of primary response genes (PRGs) or IEGs, which respond to stimuli in minutes without requiring de novo protein synthesis. The latter wave, known as secondary response genes (SRGs), largely depends on IEG-mediated transcription. Brief activity induces only PRGs, while sustained activity used in the ChIP-seq and nascent RNA-seq experiments is able to induce both neuronal IEG transcription and the second wave of SRG transcription.[53] The potential implications of the KCl duration discrepancy exist but are unlikely to affect the conclusion of this study. Although KCl concentrations are positively correlated with membrane voltage, signal strength may not be linearly correlated with Ca2+ influx levels.[25] Application of 10 mM KCl or higher leads to spontaneous neuronal activity arrest and triggers IEG transcription.[25,65] The discrepancies in concentration and duration may explain why we identified only 26 potential eRNAs. Some activity-regulated eRNAs may have been missed due to the different concentrations and durations of KCl treatment. However, it is unlikely that the differences would change the identification of these 26 activity-regulated eRNAs. Importantly, this study presented a multiomics approach for eRNA analysis and highlighted the higher sensitivity of nascent RNA-seq in detecting potential eRNAs compared to total RNA-seq.

CONCLUSIONS

In summary, our study highlights the advantages of using nascent RNA-seq labeled by the cell-type-specific UPRT−5EUracil method for identifying low-abundance lncRNAs, particularly eRNAs. Our results demonstrate that nascent RNA-seq, when enriched with the H3K27ac signal, can effectively identify potential eRNAs in response to membrane depolarization with high resolution. These findings can help uncover the role of eRNA-mediated gene activation networks in neuronal systems, providing valuable insights into the molecular processes that underlie neurological diseases. Furthermore, we developed a new bioinformatic framework for detecting eRNAs, which we have made available to the scientific community. e-finder can facilitate the detection of eRNAs in a broader range of applications.

METHODS

Cortical Neuron Culture. Dissociated primary neuron cultures were prepared from embryonic day 18 (E18) C57BL/6 embryonic mouse cortical tissue using a protocol established previously.[20] Briefly, cortices were immediately dissected and then gently dissociated with papain (Sangon Biotech #A003124) and benzonase nuclease (Beyotime #D7121-25KU) for 20 min at 37 °C. To generate single neuron suspension, primary neurons strained through a sterile 40 μm cell strainer (BD Falcon #352340) were seeded in a 6-well culture plate precoated overnight with poly L-lysine at a density of 1 million cells per well and culture medium was added to the wells. Neurons were plated in neurobasal medium (GIBCO #21103049) plus 2% B-27 (GIBCO #17504044), 1% penicillin/streptomycin (NCM Biotech #C125C8), and 1% GlutaMAX (GIBCO #35050061) at 37∘C. The medium was changed every 1−2 days, and neurons were grown until the day in vitro 7 (DIV7). On DIV8, neurons were stimulated within media supplemented with KCl (20 mM) or vehicle, and RNA was extracted directly after 0, 1, 3, 5, 7, and 12 h of the treatment. This animal study was approved by the Ethics Committee of the Zhongnan Hospital of Wuhan University.

RNA Extraction and RT-qPCR. RNA was extracted from neurons collected at different time points (0, 1, 3, 5, 7, and 12 h) after KCl stimulation using RNAiso Plus reagent (Takara). The extracted RNA was then quantified using Nanodrop and reverse-transcribed into cDNA with HiScript II Reverse Transcriptase (Vazyme; 500 ng RNA per sample) according to Takara's protocol. RT-derived cDNA was then subject to qPCR in duplicate for each sample with SYBR-Green Master Mix (Qiagen) on a Rotor-Gene Q platform (Qiagen). The relative gene expression values normalized to a Pgk1 endogenous control were analyzed by using the 2-DeltaDeltaCt method. Data from biological replicates are plotted as mean ± SEM. The PCR primer sequences used in this study are shown in Table S1.

Data Sources. *H3K27ac ChIP-seq Data.* They were obtained from the Gene Expression Omnibus (GEO) database (accession number: GSE60192). The data were generated from primary cortical neurons treated with 55 mM KCl or vehicle for 2 h.[8] This data set includes two independent biological replicates for both KCl and vehicle H3K27ac ChIP-seq, as well as one matched input DNA sample.

Nascent RNA-seq and Traditional RNA-seq Data. They were generated in a previous study.[20] Nascent RNA-seq data were generated by labeling nascent RNAs for 10 min prior to a 3 h KCl stimulation period, while traditional RNA-seq data were generated

https://doi.org/10.1021/acschemneuro.4c00047
ACS Chem. Neurosci. 2024, 15, 3626−3639

from primary cortical neurons treated with 20 mM KCl or vehicle for 3 h. Each group contained four independent biological replicates. Raw sequencing data can be obtained from the corresponding authors upon request.

CBP, H3K4me1, H3K4me3, RNAPII, and H3K27me3 ChIP-seq Data. These data sets were generated from mouse embryo cortices treated with 55 mM KCl or vehicle for 2 h. For each condition, the data consist of two biological replicates for RNAPII, H3K4me1, H3K4me3, and H3K27me3. The CBP ChIP-seq data consists of one KCl and one vehicle sample. Data sets were downloaded from the GEO database (accession number: GSE21161).[6]

Other H3K27ac ChIP-seq Data. Two H3K27ac ChIP-seq data were obtained from the GEO database to ensure the reliability of the target genomic regions (accession numbers: GSE75191[66] and GSE131025[67]). The H3K27ac ChIP-seq downloaded from GSE75191[66] were derived from the primary cortical neuron treated with 50 mM KCl or vehicle for 45 min. Each group contained one sample. Another H3K27ac ChIP-seq downloaded from GSE131025[67] was derived from the primary cortical neuron treated with either 1 uM tetrodotoxin (TTX, a sodium channel blocker that inhibits neuronal firing), or 10 uM bicuculline (Bic, which increases neuronal firing by blocking GABA-mediated inhibition) for 24 h. This H3K27ac ChIP-seq data consists of one TTX, one vehicle, and one Bic sample.

H3K4me2 ChIP-seq Data. They were downloaded from the GEO database (accession number: GSE63271[34]). These data sets were generated from wide-type primary cortical neurons treated with 55 mM KCl for 1 h. Each group contains one sample.

BRG1 ChIP-seq data. They were downloaded from the GEO database (accession number: GSE174581[35]) and generated from primary cortical neurons treated with 50 mM KCl for 1 h. Each group contains one sample.

Another Activation Model. This data set includes primary cortical neurons treated with 10 nM purified recombinant Reelin for 1 h and contains samples for CBP, CREB, H3K4me2, and H3K27ac (accession number: GSE66701[36]). Each group contains one sample.

NMDA Activation Model. This data set includes H3K27ac ChIP-seq and RNA-seq profiles derived from day 10 neurons upon control and 200 μM NMDA treatment (accession number: GSE65713[68]). Each group contains two samples.

Other Traditional RNA-seq Data. For Pearson's correlation analysis, we downloaded other traditional RNA-seq data from the GEO database (accession number: GSE78688[69]). RNA-seq data were generated from primary cortical neurons treated with 55 mM KCl or vehicle for 0, 1, and 6 h. Each group contained three independent biological replicates.

ChIP-seq Data Analysis. We evaluated the quality of the raw FASTQ files using FastQC (v0.11.9). The results indicated that the raw data was of high quality, and therefore, we did not perform read trimming. The reads were then aligned to the mouse reference genome (mm10) using BWA-backtrack (v0.7.17) with default parameters.[70] The resulting alignment files were then converted to sorted BAM files, and low mapping-quality alignments were filtered out using SAMtools (v1.14)[71] with the option of "samtools view -Sbq 1". MACS2 (v2.2.7)[72] was used to call peaks with the option of "-f BAM -g mm -q 0.05 --nomodel --extsize 150 --bdg". After peak calling, regions of differential enrichment between the KCl stimulus group and the control group were identified by using the "bdgdiff" module in the MACS2 package. To exclude potential artifacts, we removed H3K27ac peaks that overlapped with the ENCODE mm10 blacklist regions[73] or regions surrounding ±1 kb of the transcription start site (TSS) of annotated mRNAs from the subsequent analysis.

Putative functional networks of differential H3K27ac peaks were annotated by performing a gene ontology (GO) analysis using clusterProfiler (v3.18.1).[74] We then used the "findMotifsGenome" function in Homer (v4.11)[75] for de novo motif discovery on differential H3K27ac peaks. To visualize the read coverage in counts per million, we created bigwig tracks from the merged BAM files. To validate whether active enhancers overlapped with other active or poised enhancer marks, we downloaded the bigwig tracks of RNAPII, CBP, H3K4me1, H3K27me3, H3K4me3, H3K4me2, and BRG1 and then used CrossMap (v0.6.3)[76] to liftover genomic coordinates to mm10. The bigwig track files were quantified and visualized using the "computeMatrix" and "plotProfile" modules in DeepTools (v3.5.1).[77]

RNA-seq Data Analysis. We assessed the quality of raw FASTQ files containing paired-end 150 bp*2 reads using FastQC (v0.11.9). Low-quality nucleotides (Phred <20) and Illumina adaptor sequences were trimmed by Trimmomatic (v0.39),[78] with the option of "ILLUMINACLIP:TruSeq3-PE-2.fa:2:30:10:3:true LEADING:3 TRAILING:3 HEADCROP:9 SLIDINGWINDOW:4:20 MINLEN:36". Trimmed reads were then mapped to the mm10 reference genome using HISAT2 (v2.2.1).[79] The output SAM files were converted to sorted BAM files, and low mapping-quality alignments were filtered out using SAMtools (v1.14).[71] The matrix of raw counts was obtained using featureCounts (v2.0.1).[80] Genes with remarkably low expression levels were removed (i.e., only kept genes with nonzero counts in at least four samples). Differential expression analysis was performed using the DESeq2 package (v1.30.1).[81] The total RNA-seq data in the same study[20] were also analyzed using the same bioinformatic pipeline for the comparison purpose. To ensure a more robust correlation analysis, which requires a larger sample size, we obtained 9 additional total RNA-seq data sets[69] and analyzed the data using the same bioinformatic pipeline. A total of 25 samples were included (0 h:11 samples; 1 h: 3 samples; 3 h: 8 samples; 6 h: 3 samples). Normalized counts from the DESeq2 matrix were corrected for batch effects using the "removeBatchEffect" function in the limma package[82] before conducting Pearson's correlation analysis.

■ ASSOCIATED CONTENT

Data Availability Statement

The ChIP-seq and RNA-seq data sets supporting the conclusions of this article are available in the GEO database (GSE60192, GSE21161, GSE75191, GSE131025, GSE63271, GSE174581, GSE66701, GSE78688, and GSE65713) [https://www.ncbi.nlm.nih.gov/geo/].

Supporting Information

The Supporting Information is available free of charge at https://pubs.acs.org/doi/10.1021/acschemneuro.4c00047.

Additional experimental details and results (ZIP)

DESeq2 results from nascent RNA-seq and total RNA-seq; H3K27ac peak annotation results; and primers used for qPCR (XLSX)

H3K27ac enrichment at target regions; binding profiles of H3K27ac, CBP, CREB, and H3K4me2 at differential H3K27ac sites in response to the Reelin treatment; identification and characterization of potential enhancer loci in response to NMDA treatment (PDF)

■ AUTHOR INFORMATION

Corresponding Authors

Wei Wei − *Brain Research Center, Zhongnan Hosptial of Wuhan University, Wuhan 430071, China; Department of Neurosurgery, Zhongnan Hospital of Wuhan University, Wuhan 430071, China*; Email: wei.wei@whu.edu.cn

Qiongyi Zhao − *Cognitive Neuroepigenetics Laboratory, Queensland Brain Institute, The University of Queensland, Brisbane, QLD 4072, Australia*; Email: q.zhao@uq.edu.au

Xiang Li − *Brain Research Center, Zhongnan Hosptial of Wuhan University, Wuhan 430071, China; Department of Neurosurgery, Zhongnan Hospital of Wuhan University, Wuhan 430071, China; Frontier Science Center for Immunology and Metabolism and Medical Research Institute, Wuhan University, Wuhan 430071, China; Sino-Italian Ascula Brain Science Joint Laboratory, Zhongnan Hosptial of*

https://doi.org/10.1021/acschemneuro.4c00047
ACS Chem. Neurosci. 2024, 15, 3626−3639

Wuhan University, Wuhan 430071, China; Email: li.xiang@whu.edu.cn

Authors

Jiazhi Jiang − *Brain Research Center, Zhongnan Hosptial of Wuhan University, Wuhan 430071, China; Department of Neurosurgery, Zhongnan Hospital of Wuhan University, Wuhan 430071, China;* orcid.org/0000-0002-0867-4208

Sha Liu − *Brain Research Center, Zhongnan Hosptial of Wuhan University, Wuhan 430071, China; Department of General Practice, Zhongnan Hospital of Wuhan University, Wuhan 430071, China*

Ziyue Xu − *Brain Research Center, Zhongnan Hosptial of Wuhan University, Wuhan 430071, China*

Shuangqi Yu − *Brain Research Center, Zhongnan Hosptial of Wuhan University, Wuhan 430071, China*

Lesheng Wang − *Brain Research Center, Zhongnan Hosptial of Wuhan University, Wuhan 430071, China*

Shengrong Long − *Brain Research Center, Zhongnan Hosptial of Wuhan University, Wuhan 430071, China*

Shengda Ye − *Brain Research Center, Zhongnan Hosptial of Wuhan University, Wuhan 430071, China; Department of Neurosurgery, Zhongnan Hospital of Wuhan University, Wuhan 430071, China*

Yu Yan − *Department of Neurosurgery, Zhongnan Hospital of Wuhan University, Wuhan 430071, China*

Hongyu Xu − *Brain Research Center, Zhongnan Hosptial of Wuhan University, Wuhan 430071, China*

Jianjian Zhang − *Department of Neurosurgery, Zhongnan Hospital of Wuhan University, Wuhan 430071, China*

Complete contact information is available at: https://pubs.acs.org/10.1021/acschemneuro.4c00047

Author Contributions

○J.J. and S.L. contributed equally to this work and shared the first authorship. X.L., Qy.-Z., and W.W. proposed the ideas and drafted the outlines. Jz.-J., Sq.-Y., and Zy.-X. performed the experiments and acquired the data. Qq-.Z., Jj.-Z., and S.L. provided technical support and supported data analysis and interpretation. Jz.-J., S.L., Qy.-Z., Ls.-W., Sr.-L., Hy.-X., Sd.-Y., and Y.Y. performed the literature search and completed the manuscript. X.L., Qy.-Z., and W.W. helped revise the manuscript and provided support in need. All authors have read and agreed to the published version of the manuscript.

Funding

This work was supported by the National Natural Science Foundation of China [Grant number 82001421] to X.L., the National Natural Science Foundation of China [Grant number 82171517] to W.W., and the Discipline Cultivation Program of Zhongnan Hospital, Wuhan University [Grant number ZNXKPY2022016] to W.W.

Notes

The authors declare no competing financial interest.

■ ACKNOWLEDGMENTS

The graphical abstract was created with biorender.com.

■ ABBREVIATIONS

eRNAs, enhancer RNAs; e-finder, enhancer RNA finder; CBP, cAMP response element-binding protein; H3K4me1, histone H3 monomethylated at lysine 4; H3K27ac, histone H3 lysine 27 acetylation; NET-seq, native elongating transcript sequencing; KCl, potassium chloride; VSCCs, voltage-sensitive calcium channels; L-VSCCs, L-type voltage-sensitive calcium channels; E18, embryonic day 18; DIV, day in vitro; GEO, gene expression omnibus; TSS, transcription start site; GO, gene ontology; IEG, immediate early gene; BDNF, brain-derived neurotrophic factor; PD, Parkinson's disease; TADs, topologically associating domains; PRGs, primary response genes; SRGs, secondary response genes

■ REFERENCES

(1) Furlong, E. E. M.; Levine, M. Developmental enhancers and chromosome topology. *Science* **2018**, *361* (6409), 1341−1345.

(2) Robson, M. I.; Ringel, A. R.; Mundlos, S. Regulatory Landscaping: How Enhancer-Promoter Communication Is Sculpted in 3D. *Mol. Cell* **2019**, *74* (6), 1110−1122.

(3) Kyzar, E. J.; Bohnsack, J. P.; Pandey, S. C. Current and Future Perspectives of Noncoding RNAs in Brain Function and Neuropsychiatric Disease. *Biol. Psychiatry* **2022**, *91* (2), 183−193.

(4) Field, A.; Adelman, K. Evaluating Enhancer Function and Transcription. *Annu. Rev. Biochem.* **2020**, *89*, 213−234.

(5) Sartorelli, V.; Lauberth, S. M. Enhancer RNAs are an important regulatory layer of the epigenome. *Nat. Struct. Mol. Biol.* **2020**, *27* (6), 521−528.

(6) Kim, T. K.; Hemberg, M.; Gray, J. M.; Costa, A. M.; Bear, D. M.; Wu, J.; Harmin, D. A.; Laptewicz, M.; Barbara-Haley, K.; Kuersten, S.; Markenscoff-Papadimitriou, E.; Kuhl, D.; Bito, H.; Worley, P. F.; Kreiman, G.; Greenberg, M. E. Widespread transcription at neuronal activity-regulated enhancers. *Nature* **2010**, *465* (7295), 182−187.

(7) Rada-Iglesias, A.; Bajpai, R.; Swigut, T.; Brugmann, S. A.; Flynn, R. A.; Wysocka, J. A unique chromatin signature uncovers early developmental enhancers in humans. *Nature* **2011**, *470* (7333), 279−283.

(8) Malik, A. N.; Vierbuchen, T.; Hemberg, M.; Rubin, A. A.; Ling, E.; Couch, C. H.; Stroud, H.; Spiegel, I.; Farh, K. K.; Harmin, D. A.; Greenberg, M. E. Genome-wide identification and characterization of functional neuronal activity-dependent enhancers. *Nat. Neurosci.* **2014**, *17* (10), 1330−1339.

(9) Carullo, N. V. N.; Phillips Iii, R. A.; Simon, R. C.; Soto, S. A. R.; Hinds, J. E.; Salisbury, A. J.; Revanna, J. S.; Bunner, K. D.; Ianov, L.; Sultan, F. A.; Savell, K. E.; Gersbach, C. A.; Day, J. J. Enhancer RNAs predict enhancer-gene regulatory links and are critical for enhancer function in neuronal systems. *Nucleic Acids Res.* **2020**, *48* (17), 9550−9570.

(10) Harrison, L. J.; Bose, D. Enhancer RNAs step forward: new insights into enhancer function. *Development* **2022**, *149* (16), dev2000398 DOI: 10.1242/dev.200398.

(11) Bhatt, D. M.; Pandya-Jones, A.; Tong, A. J.; Barozzi, I.; Lissner, M. M.; Natoli, G.; Black, D. L.; Smale, S. T. Transcript dynamics of proinflammatory genes revealed by sequence analysis of subcellular RNA fractions. *Cell* **2012**, *150* (2), 279−290.

(12) Churchman, L. S.; Weissman, J. S. Nascent transcript sequencing visualizes transcription at nucleotide resolution. *Nature* **2011**, *469* (7330), 368−373.

(13) Nojima, T.; Gomes, T.; Grosso, A. R. F.; Kimura, H.; Dye, M. J.; Dhir, S.; Carmo-Fonseca, M.; Proudfoot, N. J. Mammalian NET-Seq Reveals Genome-wide Nascent Transcription Coupled to RNA Processing. *Cell* **2015**, *161* (3), 526−540.

(14) Nojima, T.; Rebelo, K.; Gomes, T.; Grosso, A. R.; Proudfoot, N. J.; Carmo-Fonseca, M. RNA Polymerase II Phosphorylated on CTD Serine 5 Interacts with the Spliceosome during Co-transcriptional Splicing. *Mol. Cell* **2018**, *72* (2), 369−379.e4.

(15) Kwak, H.; Fuda, N. J.; Core, L. J.; Lis, J. T. Precise maps of RNA polymerase reveal how promoters direct initiation and pausing. *Science* **2013**, *339* (6122), 950−953.

(16) Core, L. J.; Waterfall, J. J.; Lis, J. T. Nascent RNA sequencing reveals widespread pausing and divergent initiation at human promoters. *Science* **2008**, *322* (5909), 1845−1848.

(17) Wissink, E. M.; Vihervaara, A.; Tippens, N. D.; Lis, J. T. Nascent RNA analyses: tracking transcription and its regulation. *Nat. Rev. Genet.* **2019**, *20* (12), 705−723.
(18) Jao, C. Y.; Salic, A. Exploring RNA transcription and turnover in vivo by using click chemistry. *Proc. Natl. Acad. Sci. U. S. A.* **2008**, *105* (41), 15779−15784.
(19) Schwalb, B.; Michel, M.; Zacher, B.; Frühauf, K.; Demel, C.; Tresch, A.; Gagneur, J.; Cramer, P. TT-seq maps the human transient transcriptome. *Science* **2016**, *352* (6290), 1225−1228.
(20) Zajaczkowski, E. L.; Zhao, Q. Y.; Zhang, Z. H.; Li, X.; Wei, W.; Marshall, P. R.; Leighton, L. J.; Nainar, S.; Feng, C.; Spitale, R. C.; Bredy, T. W. Bioorthogonal Metabolic Labeling of Nascent RNA in Neurons Improves the Sensitivity of Transcriptome-Wide Profiling. *ACS Chem. Neurosci.* **2018**, *9* (7), 1858−1865.
(21) West, A. E.; Chen, W. G.; Dalva, M. B.; Dolmetsch, R. E.; Kornhauser, J. M.; Shaywitz, A. J.; Takasu, M. A.; Tao, X.; Greenberg, M. E. Calcium regulation of neuronal gene expression. *Proc. Natl. Acad. Sci. U. S. A.* **2001**, *98* (20), 11024−11031.
(22) Yap, E. L.; Greenberg, M. E. Activity-Regulated Transcription: Bridging the Gap between Neural Activity and Behavior. *Neuron* **2018**, *100* (2), 330−348.
(23) Westenbroek, R. E.; Ahlijanian, M. K.; Catterall, W. A. Clustering of L-type Ca2+ channels at the base of major dendrites in hippocampal pyramidal neurons. *Nature* **1990**, *347* (6290), 281−284.
(24) Wheeler, D. G.; Groth, R. D.; Ma, H.; Barrett, C. F.; Owen, S. F.; Safa, P.; Tsien, R. W. Ca(V)1 and Ca(V)2 channels engage distinct modes of Ca(2+) signaling to control CREB-dependent gene expression. *Cell* **2012**, *149* (5), 1112−1124.
(25) Rienecker, K. D. A.; Poston, R. G.; Saha, R. N. Merits and Limitations of Studying Neuronal Depolarization-Dependent Processes Using Elevated External Potassium. *ASN Neuro* **2020**, *12*, No. 1759091420974807.
(26) Karin, M.; Liu, Z.; Zandi, E. AP-1 function and regulation. *Curr. Opin. Cell Biol.* **1997**, *9* (2), 240−246.
(27) Chottekalapanda, R. U.; Kalik, S.; Gresack, J.; Ayala, A.; Gao, M.; Wang, W.; Meller, S.; Aly, A.; Schaefer, A.; Greengard, P. AP-1 controls the p11-dependent antidepressant response. *Mol. Psychiatry* **2020**, *25* (7), 1364−1381.
(28) Ding, P.; Chen, W.; Yan, X.; Zhang, J.; Li, C.; Zhang, G.; Wang, Y.; Li, Y. BMPER alleviates ischemic brain injury by protecting neurons and inhibiting neuroinflammation via Smad3-Akt-Nrf2 pathway. *CNS Neurosci. Ther.* **2022**, *28* (4), 593−607.
(29) Yu, C. Y.; Gui, W.; He, H. Y.; Wang, X. S.; Zuo, J.; Huang, L.; Zhou, N.; Wang, K.; Wang, Y. Neuronal and astroglial TGFβ-Smad3 signaling pathways differentially regulate dendrite growth and synaptogenesis. *Neuromolecular Med.* **2014**, *16* (2), 457−472.
(30) Harris, H. K.; Nakayama, T.; Lai, J.; Zhao, B.; Argyrou, N.; Gubbels, C. S.; Soucy, A.; Genetti, C. A.; Suslovitch, V.; Rodan, L. H.; Tiller, G. E.; Lesca, G.; Gripp, K. W.; Asadollahi, R.; Hamosh, A.; Applegate, C. D.; Turnpenny, P. D.; Simon, M. E. H.; Volker-Touw, C. M. L.; Gassen, K.; Binsbergen, E. V.; Pfundt, R.; Gardeitchik, T.; Vries, B. B. A.; Immken, L. L.; Buchanan, C.; Willing, M.; Toler, T. L.; Fassi, E.; Baker, L.; Vansenne, F.; Wang, X.; Ambrus, J. L., Jr.; Fannemel, M.; Posey, J. E.; Agolini, E.; Novelli, A.; Rauch, A.; Boonsawat, P.; Fagerberg, C. R.; Larsen, M. J.; Kibaek, M.; Labalme, A.; Poisson, A.; Payne, K. K.; Walsh, L. E.; Aldinger, K. A.; Balciuniene, J.; Skraban, C.; Gray, C.; Murrell, J.; Bupp, C. P.; Pascolini, G.; Grammatico, P.; Broly, M.; Küry, S.; Nizon, M.; Rasool, I. G.; Zahoor, M. Y.; Kraus, C.; Reis, A.; Iqbal, M.; Uguen, K.; Audebert-Bellanger, S.; Ferec, C.; Redon, S.; Baker, J.; Wu, Y.; Zampino, G.; Syrbe, S.; Brosse, I.; Jamra, R. A.; Dobyns, W. B.; Cohen, L. L.; Blomhoff, A.; Mignot, C.; Keren, B.; Courtin, T.; Agrawal, P. B.; Beggs, A. H.; Yu, T. W. Disruption of RFX family transcription factors causes autism, attention-deficit/hyperactivity disorder, intellectual disability, and dysregulated behavior. *Genet. Med.* **2021**, *23* (6), 1028−1040.
(31) Creyghton, M. P.; Cheng, A. W.; Welstead, G. G.; Kooistra, T.; Carey, B. W.; Steine, E. J.; Hanna, J.; Lodato, M. A.; Frampton, G. M.; Sharp, P. A.; Boyer, L. A.; Young, R. A.; Jaenisch, R. Histone H3K27ac separates active from poised enhancers and predicts developmental state. *Proc. Natl. Acad. Sci. U. S. A.* **2010**, *107* (50), 21931−21936.
(32) Calo, E.; Wysocka, J. Modification of enhancer chromatin: what, how, and why? *Mol. Cell* **2013**, *49* (5), 825−837.
(33) Narita, T.; Ito, S.; Higashijima, Y.; Chu, W. K.; Neumann, K.; Walter, J.; Satpathy, S.; Liebner, T.; Hamilton, W. B.; Maskey, E.; Prus, G.; Shibata, M.; Iesmantavicius, V.; Brickman, J. M.; Anastassiadis, K.; Koseki, H.; Choudhary, C. Enhancers are activated by p300/CBP activity-dependent PIC assembly, RNAPII recruitment, and pause release. *Mol. Cell* **2021**, *81* (10), 2166−2182.e6.
(34) Wang, J.; Telese, F.; Tan, Y.; Li, W.; Jin, C.; He, X.; Basnet, H.; Ma, Q.; Merkurjev, D.; Zhu, X.; Liu, Z.; Zhang, J.; Ohgi, K.; Taylor, H.; White, R. R.; Tazearslan, C.; Suh, Y.; Macfarlan, T. S.; Pfaff, S. L.; Rosenfeld, M. G. LSD1n is an H4K20 demethylase regulating memory formation via transcriptional elongation control. *Nat. Neurosci.* **2015**, *18* (9), 1256−1264.
(35) Kim, B.; Luo, Y.; Zhan, X.; Zhang, Z.; Shi, X.; Yi, J.; Xuan, Z.; Wu, J. Neuronal activity-induced BRG1 phosphorylation regulates enhancer activation. *Cell Rep.* **2021**, *36* (2), No. 109357.
(36) Telese, F.; Ma, Q.; Perez, P. M.; Notani, D.; Oh, S.; Li, W.; Comoletti, D.; Ohgi, K. A.; Taylor, H.; Rosenfeld, M. G. LRP8-Reelin-Regulated Neuronal Enhancer Signature Underlying Learning and Memory Formation. *Neuron* **2015**, *86* (3), 696−710.
(37) Lyford, G. L.; Yamagata, K.; Kaufmann, W. E.; Barnes, C. A.; Sanders, L. K.; Copeland, N. G.; Gilbert, D. J.; Jenkins, N. A.; Lanahan, A. A.; Worley, P. F. Arc, a growth factor and activity-regulated gene, encodes a novel cytoskeleton-associated protein that is enriched in neuronal dendrites. *Neuron* **1995**, *14* (2), 433−445.
(38) Joo, J. Y.; Schaukowitch, K.; Farbiak, L.; Kilaru, G.; Kim, T. K. Stimulus-specific combinatorial functionality of neuronal c-fos enhancers. *Nat. Neurosci.* **2016**, *19* (1), 75−83.
(39) Plank, J. L.; Dean, A. Enhancer function: mechanistic and genome-wide insights come together. *Mol. Cell* **2014**, *55* (1), 5−14.
(40) Sigova, A. A.; Abraham, B. J.; Ji, X.; Molinie, B.; Hannett, N. M.; Guo, Y. E.; Jangi, M.; Giallourakis, C. C.; Sharp, P. A.; Young, R. A. Transcription factor trapping by RNA in gene regulatory elements. *Science* **2015**, *350* (6263), 978−981.
(41) Zhao, Y.; Wang, L.; Ren, S.; Wang, L.; Blackburn, P. R.; McNulty, M. S.; Gao, X.; Qiao, M.; Vessella, R. L.; Kohli, M.; Zhang, J.; Karnes, R. J.; Tindall, D. J.; Kim, Y.; MacLeod, R.; Ekker, S. C.; Kang, T.; Sun, Y.; Huang, H. Activation of P-TEFb by Androgen Receptor-Regulated Enhancer RNAs in Castration-Resistant Prostate Cancer. *Cell Rep.* **2016**, *15* (3), 599−610.
(42) Bose, D. A.; Donahue, G.; Reinberg, D.; Shiekhattar, R.; Bonasio, R.; Berger, S. L. RNA Binding to CBP Stimulates Histone Acetylation and Transcription. *Cell* **2017**, *168* (1−2), 135−149.e22.
(43) Li, W.; Notani, D.; Ma, Q.; Tanasa, B.; Nunez, E.; Chen, A. Y.; Merkurjev, D.; Zhang, J.; Ohgi, K.; Song, X.; Oh, S.; Kim, H. S.; Glass, C. K.; Rosenfeld, M. G. Functional roles of enhancer RNAs for oestrogen-dependent transcriptional activation. *Nature* **2013**, *498* (7455), 516−520.
(44) Mousavi, K.; Zare, H.; Dell'orso, S.; Grontved, L.; Gutierrez-Cruz, G.; Derfoul, A.; Hager, G. L.; Sartorelli, V. eRNAs promote transcription by establishing chromatin accessibility at defined genomic loci. *Mol. Cell* **2013**, *51* (5), 606−617.
(45) Schaukowitch, K.; Joo, J. Y.; Liu, X.; Watts, J. K.; Martinez, C.; Kim, T. K. Enhancer RNA facilitates NELF release from immediate early genes. *Mol. Cell* **2014**, *56* (1), 29−42.
(46) Tanila, H. The role of BDNF in Alzheimer's disease. *Neurobiol. Dis.* **2017**, *97* (Pt B), 114−118.
(47) Brookes, E.; Martinez De La Cruz, B.; Boulasiki, P.; Au, H. Y. A.; Varsally, W.; Barrington, C.; Hadjur, S.; Riccio, A. A novel intergenic enhancer that regulates Bdnf expression in developing cortical neurons. *iScience* **2023**, *26* (1), No. 105695.
(48) Dong, X.; Liao, Z.; Gritsch, D.; Hadzhiev, Y.; Bai, Y.; Locascio, J. J.; Guennewig, B.; Liu, G.; Blauwendraat, C.; Wang, T.; Adler, C. H.; Hedreen, J. C.; Faull, R. L. M.; Frosch, M. P.; Nelson, P. T.; Rizzu, P.; Cooper, A. A.; Heutink, P.; Beach, T. G.; Mattick, J. S.; Müller, F.;

https://doi.org/10.1021/acschemneuro.4c00047
ACS Chem. Neurosci. 2024, 15, 3626−3639

Scherzer, C. R. Enhancers active in dopamine neurons are a primary link between genetic variation and neuropsychiatric disease. *Nat. Neurosci.* **2018**, *21* (10), 1482−1492.
(49) Xu, J.; Shao, Z.; Glass, K.; Bauer, D. E.; Pinello, L.; Van Handel, B.; Hou, S.; Stamatoyannopoulos, J. A.; Mikkola, H. K.; Yuan, G. C.; Orkin, S. H. Combinatorial assembly of developmental stage-specific enhancers controls gene expression programs during human erythropoiesis. *Dev. Cell* **2012**, *23* (4), 796−811.
(50) Herrera, D. G.; Robertson, H. A. Activation of c-fos in the brain. *Prog. Neurobiol.* **1996**, *50* (2−3), 83−107.
(51) Beacon, T. H.; Delcuve, G. P.; López, C.; Nardocci, G.; Kovalchuk, I.; van Wijnen, A. J.; Davie, J. R. The dynamic broad epigenetic (H3K4me3, H3K27ac) domain as a mark of essential genes. *Clin. Epigenetics* **2021**, *13* (1), 138.
(52) Liu, X.; Wang, C.; Liu, W.; Li, J.; Li, C.; Kou, X.; Chen, J.; Zhao, Y.; Gao, H.; Wang, H.; Zhang, Y.; Gao, Y.; Gao, S. Distinct features of H3K4me3 and H3K27me3 chromatin domains in pre-implantation embryos. *Nature* **2016**, *537* (7621), 558−562.
(53) Tyssowski, K. M.; DeStefino, N. R.; Cho, J. H.; Dunn, C. J.; Poston, R. G.; Carty, C. E.; Jones, R. D.; Chang, S. M.; Romeo, P.; Wurzelmann, M. K.; Ward, J. M.; Andermann, M. L.; Saha, R. N.; Dudek, S. M.; Gray, J. M. Different Neuronal Activity Patterns Induce Different Gene Expression Programs. *Neuron* **2018**, *98* (3), 530−546.e11.
(54) Shigeyasu, K.; Toden, S.; Ozawa, T.; Matsuyama, T.; Nagasaka, T.; Ishikawa, T.; Sahoo, D.; Ghosh, P.; Uetake, H.; Fujiwara, T.; Goel, A. The PVT1 lncRNA is a novel epigenetic enhancer of MYC, and a promising risk-stratification biomarker in colorectal cancer. *Mol. Cancer* **2020**, *19* (1), 155.
(55) Lee, J.; Wu, Y.; Harada, B. T.; Li, Y.; Zhao, J.; He, C.; Ma, Y.; Wu, X. N(6) -methyladenosine modification of lncRNA Pvt1 governs epidermal stemness. *EMBO J.* **2021**, *40* (8), No. e106276.
(56) Jin, K.; Wang, S.; Zhang, Y.; Xia, M.; Mo, Y.; Li, X.; Li, G.; Zeng, Z.; Xiong, W.; He, Y. Long non-coding RNA PVT1 interacts with MYC and its downstream molecules to synergistically promote tumorigenesis. *Cell. Mol. Life Sci.* **2019**, *76* (21), 4275−4289.
(57) Zhao, T.; Ding, Y.; Li, M.; Zhou, C.; Lin, W. Silencing lncRNA PVT1 inhibits activation of astrocytes and increases BDNF expression in hippocampus tissues of rats with epilepsy by downregulating the Wnt signaling pathway. *J. Cell. Physiol.* **2019**, *234*, 16054 DOI: 10.1002/jcp.28264.
(58) Adhikari, H.; Kattan, W. E.; Kumar, S.; Zhou, P.; Hancock, J. F.; Counter, C. M. Oncogenic KRAS is dependent upon an EFR3A-PI4KA signaling axis for potent tumorigenic activity. *Nat. Commun.* **2021**, *12* (1), No. 5248.
(59) Qian, Q.; Liu, Q.; Zhou, D.; Pan, H.; Liu, Z.; He, F.; Ji, S.; Wang, D.; Bao, W.; Liu, X.; Liu, Z.; Zhang, H.; Zhang, X.; Zhang, L.; Wang, M.; Xu, Y.; Huang, F.; Luo, B.; Sun, B. Brain-specific ablation of Efr3a promotes adult hippocampal neurogenesis via the brain-derived neurotrophic factor pathway. *FASEB J.* **2017**, *31* (5), 2104−2113.
(60) Dekker, J.; Rippe, K.; Dekker, M.; Kleckner, N. Capturing chromosome conformation. *Science* **2002**, *295* (5558), 1306−1311.
(61) Lieberman-Aiden, E.; van Berkum, N. L.; Williams, L.; Imakaev, M.; Ragoczy, T.; Telling, A.; Amit, I.; Lajoie, B. R.; Sabo, P. J.; Dorschner, M. O.; Sandstrom, R.; Bernstein, B.; Bender, M. A.; Groudine, M.; Gnirke, A.; Stamatoyannopoulos, J.; Mirny, L. A.; Lander, E. S.; Dekker, J. Comprehensive mapping of long-range interactions reveals folding principles of the human genome. *Science* **2009**, *326* (5950), 289−293.
(62) Beagan, J. A.; Phillips-Cremins, J. E. On the existence and functionality of topologically associating domains. *Nat. Genet.* **2020**, *52* (1), 8−16.
(63) Rao, S. S.; Huntley, M. H.; Durand, N. C.; Stamenova, E. K.; Bochkov, I. D.; Robinson, J. T.; Sanborn, A. L.; Machol, I.; Omer, A. D.; Lander, E. S.; Aiden, E. L. A 3D map of the human genome at kilobase resolution reveals principles of chromatin looping. *Cell* **2014**, *159* (7), 1665−1680.
(64) Fowler, T.; Sen, R.; Roy, A. L. Regulation of primary response genes. *Mol. Cell* **2011**, *44* (3), 348−360.
(65) Rienecker, K. D. A.; Poston, R. G.; Segales, J. S.; Finholm, I. W.; Sono, M. H.; Munteanu, S. J.; Ghaninejad-Esfahani, M.; Rejepova, A.; Tejeda-Garibay, S.; Wickman, K.; Marron Fernandez de Velasco, E.; Thayer, S. A.; Saha, R. N. Mild membrane depolarization in neurons induces immediate early gene transcription and acutely subdues responses to a successive stimulus. *J. Biol. Chem.* **2022**, *298* (9), No. 102278.
(66) Policarpi, C.; Crepaldi, L.; Brookes, E.; Nitarska, J.; French, S. M.; Coatti, A.; Riccio, A. Enhancer SINEs Link Pol III to Pol II Transcription in Neurons. *Cell Rep.* **2017**, *21* (10), 2879−2894.
(67) Beagan, J. A.; Pastuzyn, E. D.; Fernandez, L. R.; Guo, M. H.; Feng, K.; Titus, K. R.; Chandrashekar, H.; Shepherd, J. D.; Phillips-Cremins, J. E. Three-dimensional genome restructuring across timescales of activity-induced neuronal gene expression. *Nat. Neurosci.* **2020**, *23* (6), 707−717.
(68) Thakurela, S.; Sahu, S. K.; Garding, A.; Tiwari, V. K. Dynamics and function of distal regulatory elements during neurogenesis and neuroplasticity. *Genome Res.* **2015**, *25* (9), 1309−1324.
(69) Ataman, B.; Boulting, G. L.; Harmin, D. A.; Yang, M. G.; Baker-Salisbury, M.; Yap, E. L.; Malik, A. N.; Mei, K.; Rubin, A. A.; Spiegel, I.; Durresi, E.; Sharma, N.; Hu, L. S.; Pletikos, M.; Griffith, E. C.; Partlow, J. N.; Stevens, C. R.; Adli, M.; Chahrour, M.; Sestan, N.; Walsh, C. A.; Berezovskii, V. K.; Livingstone, M. S.; Greenberg, M. E. Evolution of Osteocrin as an activity-regulated factor in the primate brain. *Nature* **2016**, *539* (7628), 242−247.
(70) Li, H.; Durbin, R. Fast and accurate short read alignment with Burrows-Wheeler transform. *Bioinformatics* **2009**, *25* (14), 1754−1760.
(71) Danecek, P.; Bonfield, J. K.; Liddle, J.; Marshall, J.; Ohan, V.; Pollard, M. O.; Whitwham, A.; Keane, T.; McCarthy, S. A.; Davies, R. M.; Li, H. Twelve years of SAMtools and BCFtools. *Gigascience* **2021**, *10* (2), giab008 DOI: 10.1093/gigascience/giab008.
(72) Zhang, Y.; Liu, T.; Meyer, C. A.; Eeckhoute, J.; Johnson, D. S.; Bernstein, B. E.; Nusbaum, C.; Myers, R. M.; Brown, M.; Li, W.; Liu, X. S. Model-based analysis of ChIP-Seq (MACS). *Genome Biol.* **2008**, *9* (9), R137.
(73) Amemiya, H. M.; Kundaje, A.; Boyle, A. P. The ENCODE Blacklist: Identification of Problematic Regions of the Genome. *Sci. Rep.* **2019**, *9* (1), No. 9354.
(74) Wu, T.; Hu, E.; Xu, S.; Chen, M.; Guo, P.; Dai, Z.; Feng, T.; Zhou, L.; Tang, W.; Zhan, L.; Fu, X.; Liu, S.; Bo, X.; Yu, G. clusterProfiler 4.0: A universal enrichment tool for interpreting omics data. *Innovation* **2021**, *2* (3), No. 100141.
(75) Heinz, S.; Benner, C.; Spann, N.; Bertolino, E.; Lin, Y. C.; Laslo, P.; Cheng, J. X.; Murre, C.; Singh, H.; Glass, C. K. Simple combinations of lineage-determining transcription factors prime cis-regulatory elements required for macrophage and B cell identities. *Mol. Cell* **2010**, *38* (4), 576−589.
(76) Zhao, H.; Sun, Z.; Wang, J.; Huang, H.; Kocher, J. P.; Wang, L. CrossMap: a versatile tool for coordinate conversion between genome assemblies. *Bioinformatics* **2014**, *30* (7), 1006−1007.
(77) Ramírez, F.; Ryan, D. P.; Grüning, B.; Bhardwaj, V.; Kilpert, F.; Richter, A. S.; Heyne, S.; Dündar, F.; Manke, T. deepTools2: a next generation web server for deep-sequencing data analysis. *Nucleic Acids Res.* **2016**, *44* (W1), W160.
(78) Bolger, A. M.; Lohse, M.; Usadel, B. Trimmomatic: a flexible trimmer for Illumina sequence data. *Bioinformatics* **2014**, *30* (15), 2114−2120.
(79) Zhang, Y.; Park, C.; Bennett, C.; Thornton, M.; Kim, D. Rapid and accurate alignment of nucleotide conversion sequencing reads with HISAT-3N. *Genome Res.* **2021**, *31* (7), 1290−1295.
(80) Liao, Y.; Smyth, G. K.; Shi, W. featureCounts: an efficient general purpose program for assigning sequence reads to genomic features. *Bioinformatics* **2014**, *30* (7), 923−930.
(81) Love, M. I.; Huber, W.; Anders, S. Moderated estimation of fold change and dispersion for RNA-seq data with DESeq2. *Genome Biol.* **2014**, *15* (12), 550.

(82) Ritchie, M. E.; Phipson, B.; Wu, D.; Hu, Y.; Law, C. W.; Shi, W.; Smyth, G. K. limma powers differential expression analyses for RNA-sequencing and microarray studies. *Nucleic Acids Res.* **2015**, *43* (7), No. e47.

https://doi.org/10.1021/acschemneuro.4c00047
ACS Chem. Neurosci. 2024, 15, 3626−3639